Investigation of MIM Structures as Selector Devices for Crossbar Memory Arrays

Peter Vowell

Abstract—As memory continues to scale further and densities continue to increase, leakage current becomes a non-trivial concern. A selector device limits the leakage current from memory elements so that the current passing through a selected device significantly exceeds the residual leakage. An MIM device can be used in conjunction with a memory element to invoke non-linear I-V characteristics. A Ni/TiO2/Ni film stack was chosen for three main reasons: a large non-linearity factor, high on/off current ratio, and bipolar switching capabilities. An on/off ratio of six orders of magnitude was observed, and current densities on the order of 10kA/cm2 were realized using devices with one-half micron feature sizes. It was shown that current density does not scale with device size, but instead increases with decreasing device area. This confirms that required current densities are realistically achievable with continued scaling.

Index Terms—IEEE, non-volatile memory, selector devices, MIM structures, crossbar memory array.

1 Introduction

COLLECTING and interpreting overwhelming amounts of information is often the key to running a successful business in our current age of technology. The birth of big data analytics means the human race is gathering more information than we ever have before. In 2015, it was reported that the world produces 2.5 exabytes of data every day, and this number has only grown since then [11]. Being able to produce information on such a scale isn't enough however - there has to be somewhere to store it all. NAND flash memory has driven an unprecedented period of prosperity and growth for solid-state and storage class memory. However, NAND flash is reaching the limits of its potential scalability, and thus there is a greater focus on researching new non-volatile memories.

Many of these new memory technologies call for dense packing in what are known as crossbar arrays. Reliably accessing memory in dense crossbar arrays requires the current passing through the selected device to greatly exceed the inevitable leakage current present in the non-selected devices. At lower densities, this hasn't been an issue manufacturers have had to attend to greatly. At high densities however, leakage current becomes a non-trivial issue that must be addressed. Creating an environment that is conducive to highly non-linear I-V characteristics is a known solution to this problem. Implementing a selector device in series with a memory element can result in the desired change in characteristics.

Metal-insulator-metal (MIM) based selectors display promising behaviors, and can be easily integrated into existing crossbar memory array production processes. Specifically, MIM devices comprised of nickel and titanium dioxide (Ni:TiO_2:Ni) show desirably high on/off current ratios and a large non-linearity factor. They are also operated via bipolar switching, a requirement for integration with Resistive RAM (RRAM) and Spin Torque Transfer Magnetic RAM (STT-MRAM).

• *P. Vowell was with the Department of Electrical and Microelectronic Engineering, Rochester Institute of Technology, Rochester, NY, 14623.*
E-mail: psvowell@gmail.com
Website: www.petervowell.com

2 Theory

2.1 Titanium Dioxide

Titanium dioxide (TiO_2) is being used as the insulating material in the MIM filmstack. The band gap of TiO_2 varies widely with the degree of crystallinity of the film. This in turn leads to variation in the differences between the work function of the electrode and the band gap of the insulator, which makes it hard to predict the exact device behavior. If TiO_2 is deposited below 200 degrees Celsius, the created film is amorphous. This was the target deposition state, as the amorphous state has the least surface topography.

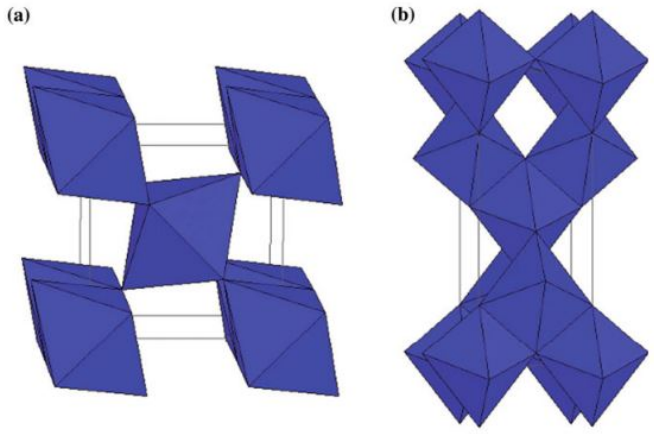

Fig. 1: Two of the most common crystalline forms of TiO_2, with **a** showing the rutile form and **b** showing the anatase form [6].

Above 240 degrees, there will be some degree of cyrstallinity to the film, in accordance with the anatase form of titanium dioxide. Above a temperature of 700 degrees, the crystalline behavior changes, and there will be some degree

of crystallinity in accordance with the rutile form of titanium dioxide [7]. Crystallization of the film can potentially lead to a better on/off current ratio for the selector device, but also decreases the functional voltage margin [1]. Crystallized films also produce more surface roughness than amorphous films, leading to larger variations in the functionality of the MIM selector device.

2.2 Schottky Emission

Due to the presence of oxygen vacancies throughout the TiO_2 lattice, TiO_2 is considered an n-type semiconductor [6]. In the $Ni/TiO_2/Ni$ selector devices referenced in this paper however, the oxygen vacancies are thought to play little part in the actual current emission. Instead, emission across the Schottky barrier at the Ni/TiO_2 interface is the main mechanism responsible for the flow of current. Knowing this, the thermionic emission current can be defined as:

$$J_s = A^* T^2 exp\left(\frac{-(q\phi_n)}{kT}\right) \tag{1}$$

where J_s is the saturation current, $A*$ is the Richardson constant, T is the temperature in Kelvin, q is the fundamental electron charge, ϕ_n is the barrier height, and k is Boltzmann's constant.

The emission is not only dependent on temperature, but on the electric field as well. Introducing an electric field can drive electrons away from the surface, effectively decreasing the barrier height. This change in work function can be modeled by:

$$\Delta\phi_n = \sqrt{\frac{q\mathcal{E}}{4\pi\epsilon_s}} \tag{2}$$

where $\mathcal{E}$ is the induced electric field, and ϵ_s is the relative permittivity of the material (in this case TiO_2). If $\Delta\phi_n$ is considered, the equation for the thermionic emission current becomes:

$$J_s = A^* T^2 exp\left(\frac{-(q\phi_n - \Delta\phi_n)}{kT}\right) \tag{3}$$

Equation three adequately explains the emission over the Ni/TiO_2 barrier.

2.3 Selector Device Explanation

As the density of crossbar memory continues to increase, the leakage current from unselected cells becomes an extremely pressing matter. To solve this problem, a selector device can be integrated into the crossbar array. A selector device limits the leakage current from memory elements so that the current passing through a selected device significantly exceeds that of the residual leakage from all of the other unselected cells.

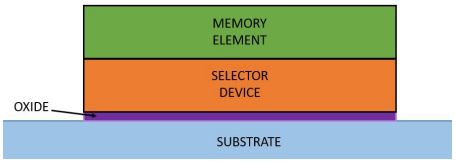

Fig. 2: Simple cross-sectional view demonstrating a selector device integrated with a memory element.

There are multiple choices for a potentially adequate selector device. Theoretically, MIM devices fulfill four of the critical selection criteria, displayed in table one.

Parameter	Ideal Value
Current Density	$\geq 10 \frac{MA}{cm^2}$
On/Off Ratio	$\geq 10^6$
Operation Polarity	Bipolar
Scalability	Compatible with Memory Element

TABLE 1: Summary of critical selection criteria for selector devices.

Previous works have shown high on/off ratios that enable the required non-linear characteristics, as well as reliable bipolar operation over a high number of cycles [12] [13]. This work will show that appropriate current densities are achievable with further device scaling.

3 Experimental Details

3.1 Mask Design

Before processing could begin, a lithographic mask had to be designed. The design phase was carried out with a strict emphasis on testing abilities. There are six different 3 by 3 crossbar arrays, varying in size from 16 micron features down to one-half micron features. The feature size was solely limited by the abilities of the manufacturing technology available during the length of this study. There are also isolated selector devices of each alloted size. This allows for an analysis of the differences between isolated cells and cells that are contained within an array.

It is important to note that while the crossbar array itself is a relatively small structure, it requires a large supporting apparatus in order to enable a simple testing scheme. Testing was performed with an HP 4145b semiconductor parameter analyzer that utilizes a 12-probe layout. This limited crossbar arrays to 3 by 3, so that testing could be semi-automated. A close look at a one-half micron crossbar array can be seen in figure three, and the overall mask structure for a single die can be seen in figure four.

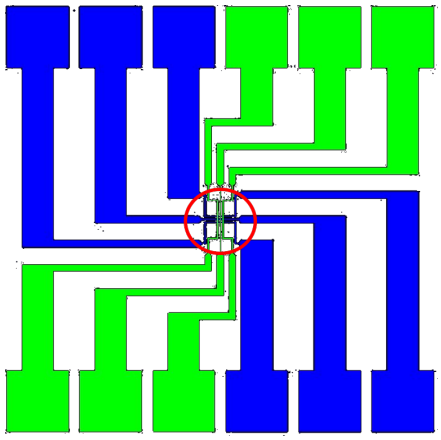

Fig. 3: Close-up of the layout for a $\frac{1}{2}$ micron crossbar array. The actual crossbar array is contained within the red circle; the rest of the visible apparatus exists for testing purposes.

Van Der Pauw structures were included for both metal films, for the purpose of measuring and comparing the sheet resistance of each nickel layer. Lines of varying widths were also included within the design, enabling confirmation of deposition thicknesses.

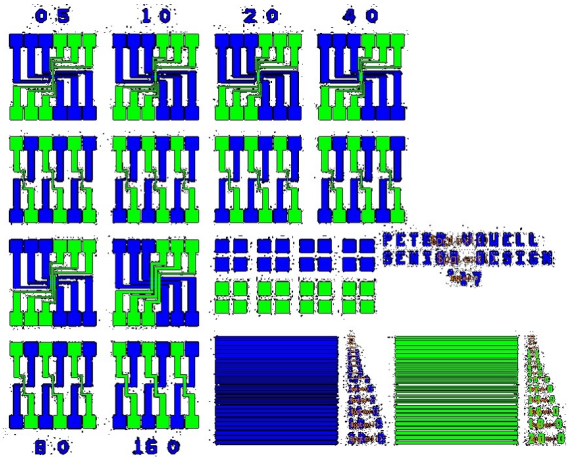

Fig. 4: Overall layout for a single die on the lithographic mask.

3.2 Process Flow

The entire manufacturing process for the specified MIM crossbar device required only nine steps. The TiO_2 is self-aligned by the lithographic step meant for patterning the top electrode, so only two lithographic steps are needed. The process flow used should easily integrate into pre-existing crossbar array processes, allowing for a minimal decrease in processing time when merging selector device manufacturing with that of a non-volatile memory element.

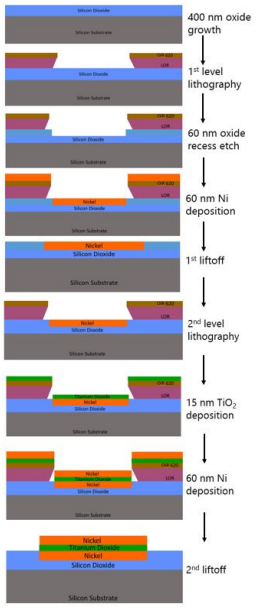

Fig. 5: Nine-step process flow for selector device fabrication.

Before manufacturing of the device begins, 400 nanometers of oxide is grown as an isolation layer. The first level of lithography is then performed, in order to pattern the bottom electrode. Before the nickel is deposited however, a 60 nanometer recess is etched into the grown oxide. There were concerns about TiO_2 potentially coating the side of the bottom electrode upon deposition, leading to undesirable current dispersion during device operation. A recess for the first metal layer was decided upon as a solution for this concern. Then the first nickel layer is deposited via electron beam evaporation, and liftoff is performed, only leaving nickel in the recessed areas. The second level of lithography is then performed, after which the titanium dioxide is deposited. The top electrode is deposited next, and another liftoff step reveals fully functional selector devices.

3.3 Process Development

After the mask was designed and the processing steps were decided upon, fabrication of the device began. The original plan was to use atomic layer deposition (ALD) for the titanium dioxide film. However, due to a combination of unforeseen issues with the ALD tool and some uncontrollable time constraints, only one attempt was made at using ALD. Unfortunately, the nickel for the bottom electrode experienced cracking from stress almost instantly upon placement within the ALD system. For the remaining process wafers, the same electron beam evaporation tool used to deposit the nickel was utilized to deposit TiO_2. Due to this change, the thermal budget increased, and the TiO_2 should have deposited in a semi-crystalline rutile form, rather than the amorphous form that was anticipated. SEM images were to be taken in order to confirm this, but due to a variety of issues that arose with the SEM tools, this could not be completed.

3.3.1 Nickel Cracking

When the wafer was placed on the hotplate within the ALD tool, the plate was heated to 120 degrees Celsius. Within twelve seconds, the nickel in place for the bottom electrode began to visibly crack from heat-induced stress.

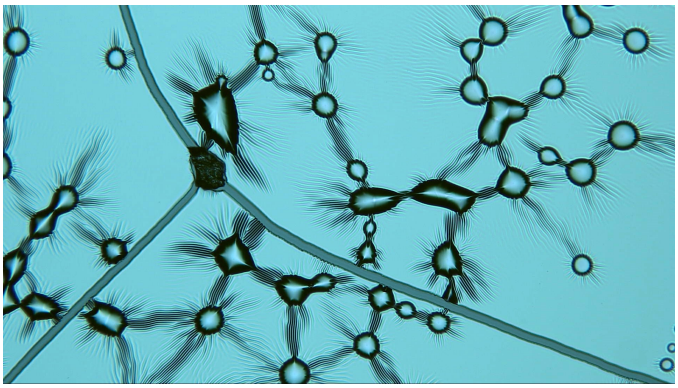

Fig. 6: Cracking of nickel from heat-induced stress.

In the future, titanium dioxide deposition via ALD could be attempted again by significantly lowering the initial hotplate temperature within the ALD tool and then slowly increasing the heat while the wafer is under vacuum in the chamber.

3.3.2 Liftoff

The first attempt at the liftoff procedure for the nickel bottom electrode yielded poor results. The liftoff procedure was performed with MicroChem's Nano Remover PG solvent.

An initial liftoff time of five hours was used, but this proved to be too short, and led to the resist scumming observed in figure seven.

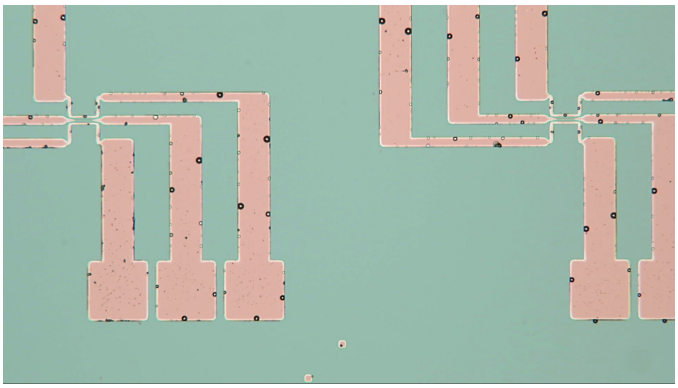

Fig. 7: Resist scumming from liftoff procedure after five hours.

The liftoff time was then increased to 22 hours, which proved long enough to entirely remove the resist without inducing any noticeable damage.

4 Results

Devices were fabricated successfully, and both crossbar arrays and isolated devices were tested. Figure eight shows current density versus voltage for a device with one-half micron features, a device with one micron features, and a device with two micron features. A maximum current density of 10 $\frac{kA}{cm^2}$ was achieved. It is notable that the current density does not scale with device size. Instead, the current density actually increases with decreasing device area. This is an important finding, as it means that the high current densities desired should be easily achievable as device area continues to decrease.

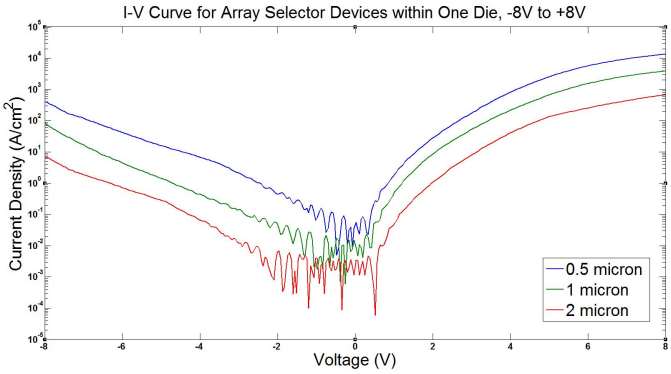

Fig. 8: Current density vs. voltage for devices with $\frac{1}{2}$ micron, 1 micron, and 2 micron feature sizes. Note that current density increases as device area decreases.

There is a clear non-linearity present in the I-V characteristics, which is desirable for a selector device. There is also a noticeable asymmetry present in the I-V curve. It is suspected that this is due to the oxidation of the bottom nickel electrode. As nickel oxidizes, the work function of the material increases, thus shifting the band diagram away from ideal and causing an asymmetry as seen here [10].

The differences in performance between cells contained within a single crossbar array was also analyzed. All cells were expected to behave similarly, due to the fact that only one device was being activated at any given time. However, this proved not to be the case. Selector devices at the center of an array yielded the best results by far, as can be discerned from figure nine.

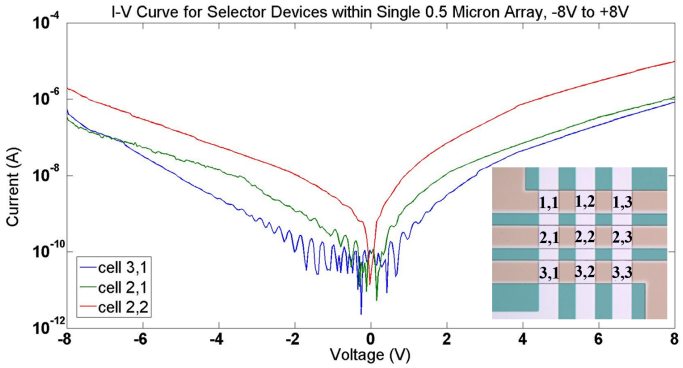

Fig. 9: I-V characteristics of individual cells within a crossbar array. Cells with fewer neighboring cells appear to perform worse.

The response of the center device is centered at zero, with an on/off ratio of almost six orders of magnitude. As testing moved further from the center and cells had fewer neighboring cells, device performance started to suffer. Specifically, the voltage margin increased, the on/off ratio decreased, and non-negligible noise was noticed in the off state. The corner cells of the crossbar array displayed the worst results, with a large voltage margin and large fluctuations in the off-state current. The results displayed in figure nine suggest that as the cell density increases, the selector device characteristics improve.

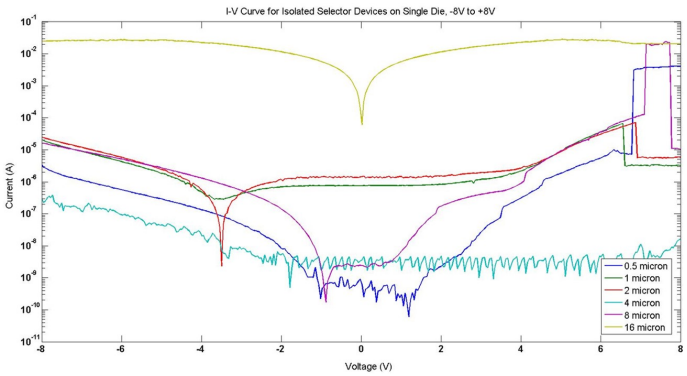

Fig. 10: I-V characteristics of isolated selector devices. Cells display extremely poor device behavior regardless of device area.

These results are confirmed by analyzing the performance of isolated cells. Figure ten shows isolated cells of varying feature sizes, all of which show extremely poor device behavior. This enhances the suspicion that cell density is tied to device performance. It is suspected that this is likely linked to stress induced during the liftoff procedure. Isolated cells could potentially be experiencing more stress

from the surrounding material during liftoff than a cell contained within a dense area. A larger investigation is needed in order to confirm this concept.

5 Conclusion

A testing die for a selector device was designed and implemented on a lithographic mask. A process was designed for the creation of a $Ni/TiO_2/Ni$ selector, and this process flow was then implemented successfully to create fully functional devices. An on/off ratio of six orders of magnitude was observed. A maximum current density of 10 kilo-amps per centimeter squared was realized, which is below the ideal value. However, it was found that current density increases with decreasing device area, leading to the conclusion that low current density will not remain an issue as device scaling continues. It was also found that as cell density increases, the device characteristics improve, which could possibly be an artifact of stress induced during the liftoff procedure. A larger investigation is needed in order to confirm this theory.

Acknowledgments

A large thank you to my advisor Dr. Santosh Kurinec, for her continual support and guidance during this project. I also want to thank Dr. Fuller, for reminding me that education can still be an enjoyable endeavor at times. Thank you to Dr. Pearson and Dr. Ewbank for their input throughout the senior design process. And thank you to the SMFL staff for ensuring the laboratory ran as smoothly as possible.

Appendix A
Resist Profiling

Initially, nLOF 2020 was chosen to be used as the photoresist for this project. The liftoff procedure was well established within the SMFL facilities, and copious amounts of documentation was available. During the length of this endevour however, nLOF 2020 was unavailable for use, and so an alternative photoresist was sought. AZ 1518 resist was tested, however the stock available in the laboratory was too old to produce an effective liftoff profile. Project budgeting did not allow for the purchase of new AZ 1518, and as such it was ruled out as a potential resist. AZ 5214 was tested next, but multiple experimental process runs led to the belief that it was a poor resist choice for the purposes of this project. The final photoresist choice was a dual system combining the photo-inactive LOR5A resist with the photo-active OiR 620. This option yielded the required liftoff profile, and was ultimately implemented to create the devices analyzed in this paper. An SEM image of the photoresist stack can be seen in figure 11.

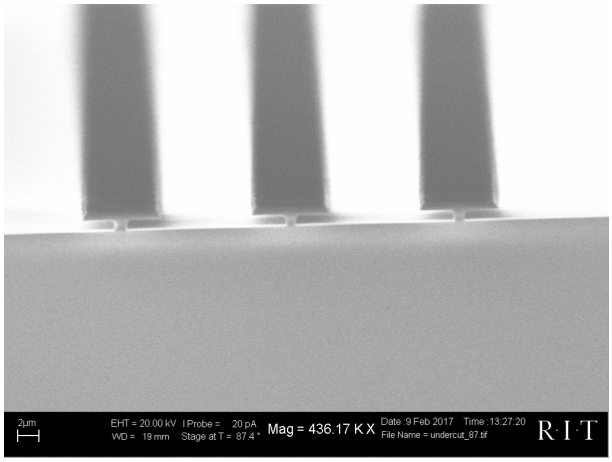

Fig. 11: SEM image of the desired resist profile.

It should be noted that the experimental resist profile shown was over-developed. A 20 second reduction in development time led to a an acceptable profile with more appropriate undercutting.

References

[1] Geoffrey W. Burr, Rohit S. Shenoy, Kumar Virwani, Pritish Narayanan, Alvaro Padilla, Blent Kurdi, Hyunsang Hwang, *Access devices for 3D crosspoint memory*, San Jose, California: IBM Research, Pohang, South Korea: Pohang University of Science and Technology, 2014.

[2] Rakesh Aluguri, Tseung-Yuen Tseng, *Overview of Selector Devices for 3-D Stackable Cross Point RRAM Arrays*, Hsinchu, Taiwan: National Chiao Tung University, 2016.

[3] Wilkie Olin-Ammentorp, *Investigation of Reactively Sputtered Titanium Oxide Memristors*, Rochester, New York: Rochester Institute of Technology, 2015.

[4] S. Kurinec, *Metal-Semiconductor Junction Surface State Heterojunctions*, Rochester, New York: Rochester Institute of Technology, 2015.

[5] L. Dommelen, *Thermionic Emission*, Tallahassee, Florida: Florida A&M University, 2002.

[6] Juan M. Coronado, Fernando Fresno, Mara D. Hernndez-Alonso, Raquel Portela, *Design of Advanced Photocatalytic Materials for Energy and Environmental Applications*, Madrid, Spain: Institute IMDEA Energa, Madrid, Spain: CIEMAT, Madrid, Spain: Institute of Catalysis and Petrochemistry, Nova Gorica, Slovenia: University of Nova Gorica.

[7] Yujian Huang, Gregory Pandraud, Pasqualina M. Sarro, *Characterization of low temperature deposited atomic layer deposition TiO2 for MEMS applications*, Delft, The Netherlands: Delft University of Technology, 2012.

[8] Simone Cortese, Ali Khiat, Daniela Carta, Mark E. Light, Themistoklis Prodromakis, *An amorphous titanium dioxide metal insulator metal selector device for resistive random access memory crossbar arrays with tunable voltage margin*, Southampton, United Kingdom: University of Southampton, 2016.

[9] Luiz G. Ferreira, Lara K. Teles, Marcelo Marques, *Band structure of NiO revisited*, São Paulo, Brazil: Instituto Tecnológico de Aeronáutica, 2009.

[10] Mark T. Greiner, Michael G. Helander, Zhi-Bin Wang, Wing-Man Tang, Zheng-Hong Lu, *Effects of Processing Conditions on the Work Function and Energy-Level Alignment of NiO Thin Films*, Toronto, Ontario, Canada: University of Toronto, 2010.

[11] IBM. Software Services Division, *Bringing big data to the enterprise*, 2016. [Online]. Available: https://www-01.ibm.com/software/data/bigdata/what-is-big-data.html. [Accessed: 03- Feb- 2017].

[12] Jiun-Jia Huang, Yi-Ming Tseng, Wun-Cheng Luo, Chung-Wei Hsu, Tuo-Hung Hou, *One selector-one resistor (1S1R) crossbar array for high-density flexible memory applications*, Hsinchu, Taiwan: National Chiao Tung University, 2011.

[13] Jiun-Jia Huang, Yi-Ming Tseng, Chung-Wei Hsu, Tuo-Hung Hou, *Bipolar Nonlinear Ni/TiO2/Ni Selector for 1S1R Crossbar Array Applications*, Hsinchu, Taiwan: National Chiao Tung University, 2011.

Peter Vowell Peter Vowell completed coursework for a B.S. in Microelectronic Engineering from Rochester Institute of Technology in May of 2017. In 2014, he co-oped as a memory quality analyst for IBM in Poughkeepsie, where he worked on NAND flash and new emerging non-volatile memory technologies. Peter began full-time employment with Epic as a technical problem solver in July of 2017. He also continues to work part-time as a freelance technical writer and contract research engineer.